ChemComm

COMMUNICATION

View Article Online
View Journal | View Issue

Cite this: *Chem. Commun.*, 2025, **61**, 18810

Received 9th September 2025,
Accepted 23rd October 2025

DOI: 10.1039/d5cc05206h

rsc.li/chemcomm

Tuneable phosphorescence and singlet oxygen production of bridged ethers *via* chalcogen variation and photocyclisation

Marco Schmiedtchen, †[a] Sidharth Thulaseedharan Nair Sailaja, †[a] Rick Y. Lorberg, †[a] Christoph Wölper,[b] Anzhela Galstyan [c] and Jens Voskuhl *[a]

In this contribution, we merged a motif for solution and solid-state emission (SSSE) with thioethers capable of photocyclisation to combine efficient emission across several states of aggregation with tuneable phosphorescence. In addition, the bridged ethers revealed remarkable singlet oxygen quantum yields that increase with the chalcogen's atomic number.

The coinage of the aggregation induced emission (AIE) effect by Tang in 2001[1] marks the beginning of an extensive research endeavour into the aggregation-dependent emission behaviour of luminophores.[2] As the diametric opposite of aggregation-caused quenching (ACQ), AIEgens deliver decisive advantages for widespread applications in fields such as chemical sensing,[3] biological probes[4] or optoelectronics.[5] Since then, AIE research has not only shaped the landscape of luminophore design, but also led to the discovery of nuanced phenomena between the extremes.[6,7] By connecting typical ACQ and AIE structures, novel compounds that provide solution and solid-state emission (SSSE) were found.[8] In addition, non-classic SSSE luminophores[9] were developed, which inherently merge planar domains with partially flexible groups to create entirely new motifs.[10] For instance, pentacene-derived bridged ethers were found to effectively handle the balance between planarity in solution and stacking prevention in the solid-state.[11] This fine-tuned interplay enabled staggering quantum yields of 32% in solution and 20% in the solid-state for a single compound.[11]

Compared to purely fluorescent samples, phosphors are even more desirable for certain applications such as bioimaging[12] or anti-counterfeiting[13] due to the delayed emission and characteristic decay. In organic phosphors, the dibenzothiophene (DBT) motif is frequently employed for its efficient intersystem crossing (ISC)[14] and good charge transport.[15] The fused ring system can be flexibly synthesised in many ways, including the photocyclisation of thioethers that produces highly substituted DBTs.[16,17] However, their emission is typically limited to the solid-state, hindering applications in solution.[14,16]

In general, the spin-forbidden ISC from singlet to triplet states can be facilitated by the inclusion of heavy atoms thanks to stronger spin–orbit-coupling (SOC).[18] Although the phosphorescence quantum yield benefits from the heavy atom effect, the excited state lifetime simultaneously decreases since the deactivation of the triplet state is also accelerated.[14] Furthermore, the presence of triplet molecular oxygen is generally detrimental to phosphorescence. The energy of the excited triplet state can be transferred to the triplet oxygen ($^3O_2$) molecule to generate singlet oxygen ($^1O_2$).[19] While this quenching process is an undesired side effect in luminescence applications, photodynamic therapy (PDT) purposely utilises the singlet oxygen for treatments against cancer[20] or antibiotic-resistant bacteria.[21]

In this contribution, we tweaked the AIE and phosphorescence properties of a selection of photocyclisable[16] bridged ethers (Fig. 1). By combining the known SSSE motif of bridged ethers[11] with thioethers, complex fused ring systems are obtained, which overcome the previous limitations to solid-state emission and grant efficient phosphorescence. In addition, the variation of the chalcogen (O, S, Se) in the bridged moiety should influence the photophysical properties not only *via* the heavy atom effect but also due to the different geometries and subsequently altered packing behaviour and intermolecular interactions. For improved solubility, isopentoxy residues are attached to the thioethers.

[a] *Faculty of Chemistry (Organic Chemistry), Center of Medical Biotechnology (ZMB) and Center for Nanointegration Duisburg-Essen (CENIDE), University of Duisburg-Essen, Universitätsstraße 7, 45117, Essen, Germany. E-mail: Jens.Voskuhl@uni-due.de*
[b] *Faculty of Chemistry (Inorganic Chemistry) and CENIDE, University of Duisburg-Essen, Universitätsstraße 5–7, 45117, Essen, Germany*
[c] *Faculty of Chemistry, CENIDE, ZMB and Center for Water and Environment Research (ZWU), University of Duisburg-Essen, Universitätsstraße 5, 45141, Essen, Germany*
† Authors contributed equally.

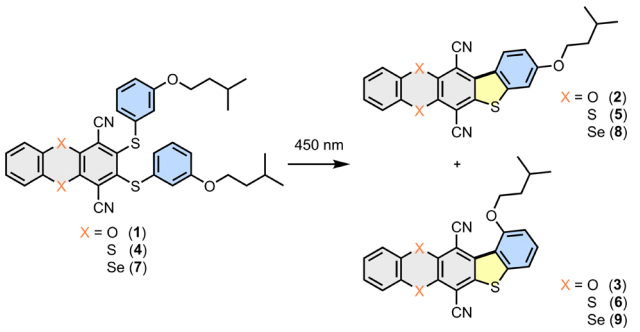

Fig. 1 Structural formulas of chalcogen bridged thioethers and dibenzothiophenes investigated in this study.

The aromatic cores were synthesised *via* two nucleophilic aromatic substitutions under basic conditions (Fig. S1). Williamson ether synthesis then granted the isopentyl ethers, which were photocyclised with 450 nm visible light. Details about the cyclisation mechanism were previously reported[16] and are discussed in the SI (Fig. S2). As expected, each thioether yielded two regioisomers, which carry the isopentoxy group in the 1- or 3-position of the DBT, respectively. All compounds were characterised with ^{1}H and ^{13}C NMR spectroscopy and high-resolution mass spectrometry (Fig. S3–S44). Additionally, single crystals of several compounds were obtained and analysed *via* X-ray diffraction (Fig. S60–S63 and Table S2).[22]

As described beforehand,[23] the bridging chalcogen alters the bending angle between the adjacent rings significantly, which can be well compared in their crystal structures. Because of the flexible alkyl chain, crystallisation of all isopentyl ethers proved to be challenging. Hence, we compare the crystal structures of the respective methyl ethers, which readily crystallised (Fig. S54–S59 and Table S1). The packing of the oxygen variant **10** reveals parallel stacking of the mostly planar (176.93(7)°) dioxin substructures in a head to tail orientation with extensive π–π contacts. In contrast, the sulfur compound **11** displays a bending angle of 140.08(7)°, which prevents planar stacking. Similarly, the selenium derivative **12** is bent even more (131.54(7)°) and lacks significant π–π interactions.

As expected from earlier iterations,[16,17] the photocyclisation causes a hypsochromic shift in the emission due to the rigidification of the molecules, which results in smaller Stokes shifts. Consequently, this effect is most pronounced in solution (Fig. S65–S68 and Table S3). Furthermore, the induced restriction of intramolecular motion (RIM) enhances the overall emission of the DBTs compared to the thioethers. For example, the quantum yield of the oxygen bridged thioether **1** in THF solution is less than 2%, while its photoproducts **2** and **3** achieve values of 11 and 7%, respectively (Fig. 2A and Table 1). In contrast, this trend is reversed in the solid-state (**1**: Φ_{PL} = 9%, **2**: Φ_{PL} = 3%, **3**: Φ_{PL} = 5%), presumably caused by increased π–π stacking in the planarised products.

Based on this observation, an aggregation study was conducted with the sulfur bridged thioether **4** and its DBT congeners **5** and **6** in mixtures of water and THF (Fig. 2B, C and Fig. S69–S71). In accordance with the intramolecular rotors

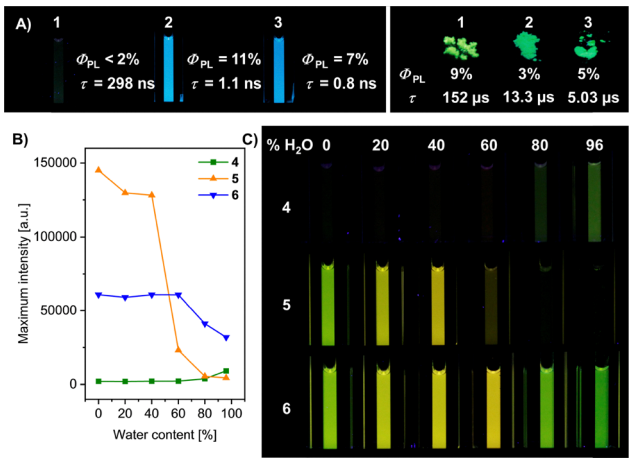

Fig. 2 (A) Photographs under 365 nm UV light, quantum yields (Φ_{PL}) and amplitude-weighted average lifetimes (τ) of compounds **1–3** in THF solution and the solid state. (B) Emission intensity of compounds **4–6** in water/THF mixtures. (C) Photographs of compounds **4–6** in water/THF mixtures under 365 nm UV light.

Table 1 Photoluminescence quantum yields (Φ_{PL}) and amplitude-weighted average lifetimes (τ) of compounds **1–9** in THF solution at r.t., solid state at r.t. and frozen 2-Me-THF solution at 77 K. Raw time-resolved photoluminescence decays, including the individual fitting components and their relative amplitudes, are available in Fig. S77–S110

	Φ_{PL} ± 0.02 solution	Φ_{PL} ± 0.02 solid state	τ [ns] solution	τ [µs] solid state	τ [ms] glassy matrix
1	<0.02	0.09	297.8 ± 0.5	152 ± 1	151.0 ± 0.6
2	0.11	0.03	1.130 ± 0.004	13.3 ± 0.2	1135 ± 4
3	0.07	0.05	0.829 ± 0.004	5.03 ± 0.06	1085 ± 3
4	<0.02	0.11	416.6 ± 0.8	131 ± 2	70.7 ± 0.3
5	0.11	0.02	2.298 ± 0.007	1392 ± 12	280.4 ± 0.2
6	0.08	0.03	1.756 ± 0.005	3100 ± 26	200.3 ± 0.3
7	<0.02	0.09	392 ± 1	545 ± 4	4.035 ± 0.007
8	<0.02	<0.02	382 ± 1	2224 ± 24	6.68 ± 0.01
9	<0.02	<0.02	377.4 ± 0.8	2209 ± 26	3.85 ± 0.02

present in **4**, the emission is quenched (Φ_{PL} < 2%) until aggregation occurs at high water concentrations. However, even at 96% water content, the compound displays only weak AIE with a quantum yield of 3%. This may indicate unfavourable packing modes inside the aggregates including π–π contacts. The 3-substituted DBT **5** exhibits ACQ: while a good quantum yield of 11% is achieved in pure THF, the emission deteriorates upon aggregation (Φ_{PL} = 2%). On the other hand, the 1-isomer **6** shows a balanced emission behaviour across all water/THF mixtures. The corresponding quantum yields of 8% (v/v = 0/100) and 5% (v/v = 96/4) qualify this compound as an SSSE.[9]

The behaviour of both isomers matches the observation of solid state and solution emission of the oxygen derivatives. Thus, it seems that the packing of the 1-isomer may generally involve less π–π stacking, allowing it to preserve its emission better even in the aggregated state.

In solution, all samples are fluorescent with lifetimes in the nanosecond regime (Table 1).[24] In this state, triplet states are

typically quenched by rotovibrational relaxation and collisions with other molecules, particularly molecular oxygen (*vide infra*). In the solid state, the lifetimes of all species range from 5 μs (**3**) to several milliseconds (**6**, **8**, **9**) corresponding to phosphorescence. Counterintuitively, the lifetimes are longer for the heavier chalcogens, which at first seems to contradict the heavy atom effect. However, this tendency could be explained with the bending angles: analogous to compound **10** (*vide supra*), the oxygen derivatives may tend to denser packings with more π–π contacts, which would favour rapid radiationless deactivation of the triplet state and a shorter lifetime for compounds **2** and **3**. A more detailed discussion is presented in the SI (Table S6). For the sulfur and selenium variants, the photocyclisation markedly prolongs the lifetime thanks to the newly formed DBT moiety.

Naturally, phosphorescence is enhanced in frozen matrices at 77 K due to minimised molecular motion and hindered collisions, allowing all the investigated compounds to phosphoresce (Fig. S73–S75). Here, the lifetimes align with the heavy atom effect. Comparing the thioethers for example (Fig. 3A and Table 1), the lifetime decreases from 151 ms (**1**, oxygen) to 71 ms (**4**, sulfur) and 4 ms (**7**, selenium). Again, a striking improvement in the lifetimes is observed after cyclisation. The oxygen bridged DBTs **2** and **3** possess impressively long amplitude-weighted average lifetimes of 1135 and 1085 ms, respectively. Remarkably, a distinct separation between fluorescence and phosphorescence is observed for these two compounds (Fig. 3B, Fig. S74). Upon excitation (λ_{ex} = 373 nm), blue fluorescence around 460 nm is visible, followed by green to yellow phosphorescence around 530–540 nm.

Notably, only the lighter oxygen derivatives show both fluorescence and phosphorescence bands with comparable relative intensity, whereas the heavier homologues predominantly exhibit phosphorescence, as expected.

To make use of the photocyclisation reaction and the phosphorescent properties of the photoproducts, compound **1** was incorporated into PMMA (poly(methyl methacrylate)) films containing 1 wt% of luminophore. These doped films were used to inscribe an image, using a photomask and blue or UV light (for the preparation procedure, see the SI). The inscribed images could be read out under UV light. The irradiated areas appear brighter because of the stronger luminescence of the photoproducts and show long afterglow, visible by eye (Fig. 3C).

Considering the strong presence of phosphorescence in the heavier chalcogen derivatives and the known correlation between efficient ISC and singlet oxygen generation, we investigated whether the enhanced SOC in sulfur (ζ_o = 365 cm^{-1}) and selenium (ζ_o = 1659 cm^{-1}), relative to oxygen (ζ_o = 154 cm^{-1}), translates into higher singlet oxygen sensitization efficiencies in these molecules.[18,25] To test this, singlet oxygen quantum yields (Φ_Δ) of the DBTs were determined using a series of solutions with varying concentrations of the samples, along with a reference solution of phenalenone (Φ_Δ = 1.00 ± 0.03 in ACN).[26,27] The singlet oxygen phosphorescence intensity at 1272 nm of each solution was measured, and Φ_Δ values were obtained from the slopes of the linear plots of integrated phosphorescence intensity (*I*) *versus* the fraction of light absorbed ($1-10^{-A}$) (see Fig. S75 for details). As a representative example, the results for the selenium isomers are shown in Fig. 4. In aerated ACN, Φ_Δ values of 44, 40, 58, 74, 82 and 70%

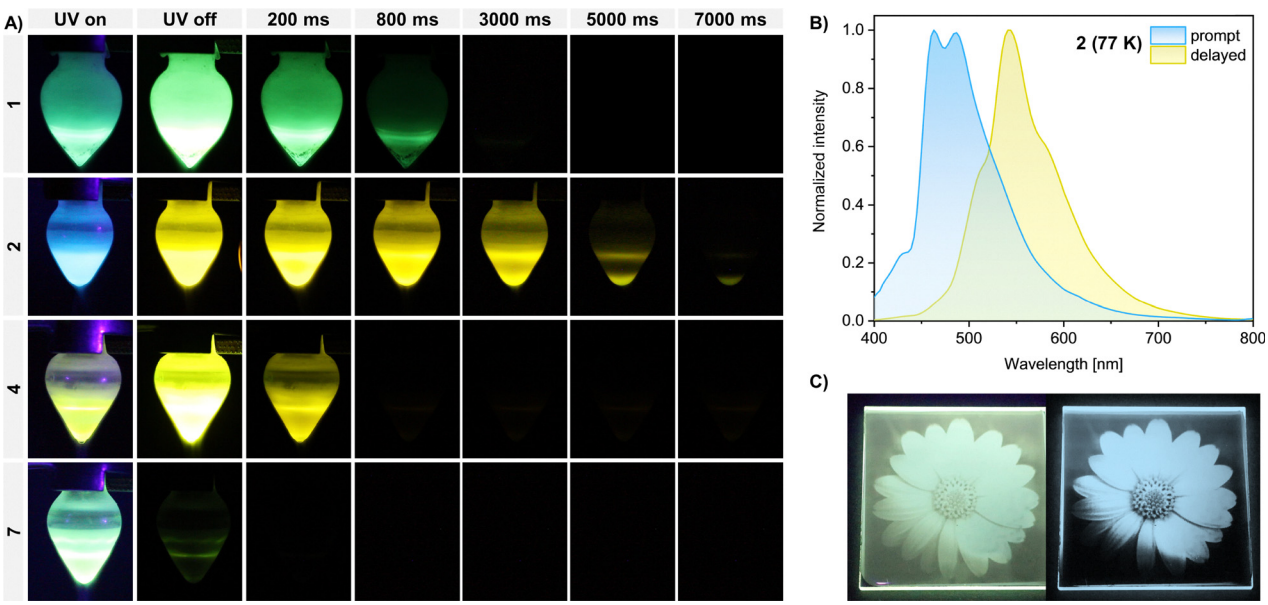

Fig. 3 (A) Photographs of compounds **1**, **2**, **4** and **7** in 2-Me-THF at 77 K under 395 nm UV light and after turning off the light source. (B) Prompt and delayed emission spectra of compound **2** in 2-Me-THF at 77 K. (C) Images of a drop-cast PMMA film doped with 1 wt% of **1**, inscribed with an image of a flower (*Osteospermum ecklonis*) into the film. The upper image shows the fluorescence of the film under 365 nm UV light, while the lower image shows the phosphorescent afterglow of the film immediately after turning off the lamp. Colour saturation of the images was adjusted so that the image represents the optical impression by eye.

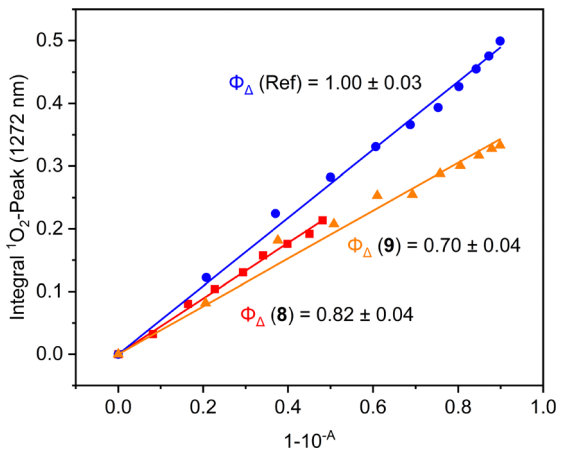

Fig. 4 Singlet oxygen photogeneration exemplarily shown for **8** and **9** in ACN. Linear regression of the integral of the $^1O_2$-peak at 1272 nm *versus* 1–10^{-A} for **8** (red), **9** (orange) and the reference phenalenone (blue). For the other compounds, see Fig. S75.

were obtained for compounds **2**, **3**, **5**, **6**, **8** and **9**, respectively (Table S7). Compared to other common photosensitizers, **8** and **9** show Φ_Δ in the upper range (see Table S8), as efficient ISC yields higher triplet populations that enable energy transfer to oxygen. Photostability tests show that **5** and **8** remain stable without decomposition upon one hour of irradiation (405 nm, 43 mW cm^{-2}), while **2** loses ~30% emission intensity (Fig. S76).

In conclusion, we have demonstrated that photocyclisable chalcogen-bridged thioethers offer a versatile platform that combines long-lived phosphorescence, efficient singlet-oxygen generation, and emission in both solution and the solid-state (SSSE). It has been demonstrated that the addition of heavier chalcogens, such as sulfur and selenium, enhances intersystem crossing, resulting in pronounced phosphorescence and high singlet oxygen quantum yields of up to 82%. These photocyclisable chalcogen-bridged luminophores demonstrate potential as a new class of materials that bridge organic phosphorescence and SSSE, with significant promise for use in photodynamic therapy and anti-counterfeiting.

We thank Søren Herkströter, Paul Kamminga and Elisabeth Verheggen for support in synthesis and crystallization and Prof. Dr. Jochen Niemeyer for providing the irradiation setup. In addition, we thank the Deutsche Forschungsgemeinschaft (DFG, German Research Foundation – Nr. 566015618) for financial support.

Conflicts of interest

There are no conflicts to declare.

Data availability

The data supporting this article have been included as part of the supplementary information (SI). Supplementary information is available. See **https://doi.org/10.1039/d5cc05206h**.

CCDC 2476381–2476386 and 2477227 contain the supplementary crystallographic data for this paper.[22a–g]

Notes and references

1 J. Luo, Z. Xie, J. W. Lam, L. Cheng, H. Chen, C. Qiu, H. S. Kwok, X. Zhan, Y. Liu, D. Zhu and B. Z. Tang, *Chem. Commun.*, 2001, 1740–1741.
2 J. Mei, N. L. C. Leung, R. T. K. Kwok, J. W. Y. Lam and B. Z. Tang, *Chem. Rev.*, 2015, **115**, 11718–11940.
3 M. Gao and B. Z. Tang, *ACS Sens.*, 2017, **2**, 1382–1399.
4 Y. Duo, Z. Xiang, G. Gao, G. Luo and B. Z. Tang, *Trends Anal. Chem.*, 2023, **167**, 117252.
5 M. Yu, R. Huang, J. Guo, Z. Zhao and B. Z. Tang, *PhotoniX*, 2020, **1**, 11.
6 Q. Zeng, Z. Li, Y. Dong, C. Di, A. Qin, Y. Hong, L. Ji, Z. Zhu, C. K. W. Jim, G. Yu, Q. Li, Z. Li, Y. Liu, J. Qin and B. Z. Tang, *Chem. Commun.*, 2007, 70–72.
7 G. Chen, W. Li, T. Zhou, Q. Peng, D. Zhai, H. Li, W. Z. Yuan, Y. Zhang and B. Z. Tang, *Adv. Mater.*, 2015, **27**, 4496–4501.
8 S. Thulaseedharan Nair Sailaja, I. Maisuls, J. Kösters, A. Hepp, A. Faust, J. Voskuhl and C. A. Strassert, *Beilstein J. Org. Chem.*, 2020, **16**, 2960–2970.
9 A. Huber, J. Dubbert, T. D. Scherz and J. Voskuhl, *Chem. – Eur. J.*, 2023, **29**, e202202481.
10 J. Shi, N. Chang, C. Li, J. Mei, C. Deng, X. Luo, Z. Liu, Z. Bo, Y. Q. Dong and B. Z. Tang, *Chem. Commun.*, 2012, **48**, 10675–10677.
11 S. Riebe, S. Adam, B. Roy, I. Maisuls, C. G. Daniliuc, J. Dubbert, C. A. Strassert, I. Schapiro and J. Voskuhl, *Chem. – Asian J.*, 2021, **16**, 2307–2313.
12 K. F. Presley, T. Falcucci, S. Shaidani, V. Fitzpatrick, J. Barry, J. T. Ly, M. J. Dalton, T. A. Grusenmeyer and D. L. Kaplan, *Biomaterials*, 2023, **301**, 122286.
13 Q. Huang, H. Gao, S. Yang, D. Ding, Z. Lin and Q. Ling, *Nano Res.*, 2020, **13**, 1035–1043.
14 W. Zhao, T. S. Cheung, N. Jiang, W. Huang, J. W. Y. Lam, X. Zhang, Z. He and B. Z. Tang, *Nat. Commun.*, 2019, **10**, 1595.
15 T.-H. Huang, W.-T. Whang, J. Y. Shen, Y.-S. Wen, J. T. Lin, T.-H. Ke, L.-Y. Chen and C.-C. Wu, *Adv. Funct. Mater.*, 2006, **16**, 1449–1456.
16 M. Schmiedtchen, I. Maisuls, H. Siera, J. Balszuweit, C. Wölper, M. Giese, G. Haberhauer, C. A. Strassert and J. Voskuhl, *Angew. Chem., Int. Ed.*, 2025, **64**, e202414326.
17 R. Y. Lorberg, S. T. Nair Sailaja, F. Terlau, M. Victoria Cappellari, M. Schmiedtchen, A. Galstyan, C. A. Strassert, M. Giese and J. Voskuhl, *Chem. – Asian J.*, 2025, **20**, e202401415.
18 A. Kremer, C. Aurisicchio, F. de Leo, B. Ventura, J. Wouters, N. Armaroli, A. Barbieri and D. Bonifazi, *Chem. – Eur. J.*, 2015, **21**, 15377–15387.
19 A. P. Castano, T. N. Demidova and M. R. Hamblin, *Photodiagn. Photodyn. Ther.*, 2004, **1**, 279–293.
20 J. Liu, F. Hu, M. Wu, L. Tian, F. Gong, X. Zhong, M. Chen, Z. Liu and B. Liu, *Adv. Mater.*, 2021, **33**, e2007888.
21 M. Vadala, D. C. Lupascu and A. Galstyan, *Photochem. Photobiol. Sci.*, 2024, **23**, 803–814.
22 (*a*) CCDC 2476381: Experimental Crystal Structure Determination, 2025, DOI: **10.5517/ccdc.csd.cc2p3w8z**; (*b*) CCDC 2476382: Experimental Crystal Structure Determination, 2025, DOI: **10.5517/ccdc.csd.cc2p3w90**; (*c*) CCDC 2476383: Experimental Crystal Structure Determination, 2025, DOI: **10.5517/ccdc.csd.cc2p3wb1**; (*d*) CCDC 2476384: Experimental Crystal Structure Determination, 2025, DOI: **10.5517/ccdc.csd.cc2p3wc2**; (*e*) CCDC 2476385: Experimental Crystal Structure Determination, 2025, DOI: **10.5517/ccdc.csd.cc2p3wd3**; (*f*) CCDC 2476386: Experimental Crystal Structure Determination, 2025, DOI: **10.5517/ccdc.csd.cc2p3wf4**; (*g*) CCDC 2477227: Experimental Crystal Structure Determination, 2025, DOI: **10.5517/ccdc.csd.cc2p4rk5**.
23 J. Dubbert, M. Valtolina, A. Huber, T. D. Scherz, C. Wölper, C. G. Daniliuc, O. Filiba, S. Sen, I. Schapiro, F. Rizzo and J. Voskuhl, *ChemPhotoChem*, 2023, **7**, e202200169.
24 B. Valeur and M. N. Berberan-Santos, *Molecular fluorescence. Principles and applications*, Wiley-VCH, Weinheim, 2nd edn, 2012.
25 M. Montalti, A. Credi, L. Prodi and M. T. Gandolfi, *Handbook of Photochemistry*, CRC Press, 2006.
26 I. Maisuls, T. M. Kirse, A. Hepp, J. Kösters, E. Wolcan and C. A. Strassert, *Inorg. Chem.*, 2022, **61**, 13775–13791.
27 S. Nonell, *Singlet Oxygen. Applications in Biosciences and Nanosciences*, Royal Society of Chemistry, Cambridge, 1st edn, 2015, vol. 1.